Available online at www.sciencedirect.com
SCIENCE DIRECT®
Thermochimica Acta 439 (2005) 127–134
thermochimica acta
www.elsevier.com/locate/tca

Thermomechanical and viscoelastic behavior of a no-flow underfill material for flip-chip applications ☆

Yi He *

Assembly Materials Characterization Laboratory, CH5-232, Intel Corporation, 5000 W. Chandler Blvd., Chandler, AZ 85226-3699, USA

Received 4 August 2005; received in revised form 22 September 2005; accepted 27 September 2005
Available online 27 October 2005

Abstract

No-flow underfill is an alternative material technology for packaging high-speed flip-chip assemblies in microelectronics industry. In this study, the thermal expansion behavior of a cured no-flow underfill material was examined by thermomechanical analysis (TMA), and the dynamic mechanical behavior was investigated by dynamic mechanical analysis (DMA) at a fixed frequency of 1 Hz. In addition, because the no-flow underfill material is polymer-based and its mechanical properties are influenced by both temperature and time, it is important to consider its viscoelastic behavior. This was accomplished by conducting the time–temperature superposition (TTS) experiments using DMA. From the TTS results, master curves were constructed for both the storage (E') and the loss moduli (E'') as a function of frequency at a pre-selected reference temperature. The shift factors along the frequency axis were also determined as a function of temperature, and they can be fitted using the Williams–Landel–Ferry (WLF) equation. Based on the master curves for E' and E'', one can obtain the relaxation modulus, $E(t,T)$, as a function of time and temperature. The measured thermomechanical and viscoelastic properties of the no-flow underfill material provided crucial material properties for accurately modeling the package stress.
© 2005 Elsevier B.V. All rights reserved.

Keywords: No-flow underfill; Viscoelasticity; Time–temperature superposition (TTS); Shift factor; Dynamic mechanical analysis (DMA); Relaxation modulus

1. Introduction

Flip-chip technology was invented by IBM over 30 years ago as an interconnect technology to package CPU chips for high performance computers [1]. In this technology, the active area of the silicon chip surface is mounted facing toward the printed circuit board (substrate) by a variety of interconnect materials and methods [2]. In a flip-chip package, an underfill encapsulant is used to fill the gap between the silicon chip and the substrate to improve the solder joint reliability.

A major concern for the flip-chip packaging technology is the thermal stress induced by the mismatch of the coefficients of thermal expansion (CTE) between the silicon chip and the substrate [3]. For example, the room temperature CTE of silicon is $\sim 2.5 \times 10^{-6}\,\mathrm{K}^{-1}$, and for the substrate, it is typically $(10\text{–}20) \times 10^{-6}\,\mathrm{K}^{-1}$ within the plane and more than $20 \times 10^{-6}\,\mathrm{K}^{-1}$ perpendicular to the plane direction. CTE mismatch-induced thermal stress can cause significant shear strain on solder joints during temperature cycling, resulting in solder fatigue and crack growth, causing premature failure of the device [4]. In order to redistribute and reduce thermal stresses on the solder joints, underfill materials are commonly used to fill the gap between the chip and the substrate [5,6].

The traditional underfilling process can be described briefly as follows: after the silicon chip is attached to the substrate through a solder reflow process, liquid underfill material, which is normally an epoxy-based material with silica filler, is dispensed along one or more sides around the perimeter of the chip, and it flows by capillary force to fill the gap between the silicon chip and the substrate. Finally, the underfill material is cured and becomes hardened. The cured underfill redistributes package stresses and can significantly reduce the stress concentration on the solder joints, thus improving device service life. Because of its strategic role, underfill material properties are crucial to package reliability performance.

☆ Presented at the 33rd NATAS Conference, Universal City, CA, USA, September 19–21, 2005, in a special Honorary Session dedicated to Professor John K. Gillham for his many contributions to the study of thermoset materials.

* Tel.: +1 480 552 3154; fax: +1 480 552 5241.
E-mail address: yi.he@intel.com.

0040-6031/$ – see front matter © 2005 Elsevier B.V. All rights reserved.
doi:10.1016/j.tca.2005.09.016

With the continuous increase in microprocessor speed and functionality and the decrease in device size, the integration of the underfill with the silicon die and the assembly processes has become a critical challenge for capillary-flow underfill materials. As a result, traditional capillary-flow underfill materials may no longer be able to meet the assembly and reliability requirements. As an alternative, no-flow underfill materials have become an attractive packaging solution.

No-flow underfill technology for flip-chip applications was initially proposed by Wong et al. to combine the soldering and underfill curing into a single reflow process [7–12]. In this technology, the no-flow underfill material, which can produce the fluxing agent by itself, is dispensed on the substrate before reflow process. This is followed by chip placement and alignment, solder reflow, and then underfill cure [9,13].

The big advantage of no-flow underfill technology over the conventional capillary-flow underfill is that the reflow and underfilling are combined into one process, so that after soldering and before the flip-chip package is cooled down to room temperature, the underfill material is already in place to reduce stress concentration on the solder joints.

In the past, the investigations into no-flow underfill technology have been mainly academic studies with low solder bump and I/O applications. In many cases the underfill material was unfilled [10–12] with typical chemical ingredients including epoxy resin, anhydride hardener, catalyst, and fluxing agent. Unfilled underfill represents a big challenge for CPU applications since its CTE is high, in the range of (60–80) $\times 10^{-6}\,K^{-1}$. From a reliability point of view, high underfill CTE is not desired because it leads to high thermal stresses in the package. To reduce the CTE of no-flow underfill, silica fillers are added, but this creates new challenges [14].

Because of the large mismatch in CTE between Si and other packaging materials, including the underfill, significant thermal stress can be induced in the package upon cooling from the assembly temperature. Therefore, the thermomechanical properties of a cured no-flow underfill, including its thermal expansion and dynamic mechanical behavior, have a major impact on package stress. In this work, thermal analysis techniques were applied to characterize the properties of a no-flow underfill candidate. The focus was on thermomechanical properties of the cured material, including its CTE, T_g, and mechanical modulus, because they are the most critical factors modulating the package stresses.

Since underfill materials are polymer-based and they are viscoelastic in nature, a pure elastic approach to estimate the thermal stress induced by temperature change is no longer appropriate. A simple example is illustrated in Fig. 1, in which we consider a pure elastic bar constrained at both ends at temperature T_1. At this temperature, the sample is not under any compressive or tensile stress, and it has an equilibrium length L. Next, the temperature is changed to T_2, which can be higher or lower than T_1. Since both ends of the bar are constrained, therefore, at T_2, the sample will experience a compressive or tensile strain ε, which is caused by thermal expansion or contraction: $\varepsilon = \alpha(T_2 - T_1) = \alpha \Delta T$, where α is the CTE of the material. The resulting stress at T_2 in the elastic bar is then $\sigma(T_2) = \varepsilon E(T_2)$, which depends only on α, ΔT, and material's Young's modulus at T_2. If the material is viscoelastic, this approach is clearly inappropriate, since stress relaxation in the material can greatly affect its stress state at T_2, especially if T_2 is close to the glass transition temperature of the material. The induced thermal stress in a viscoelastic material will not only depend on α and $E(T_2)$, but also on its glass transition temperature T_g, the rate of temperature change from T_1 to T_2, and the time spent at T_2.

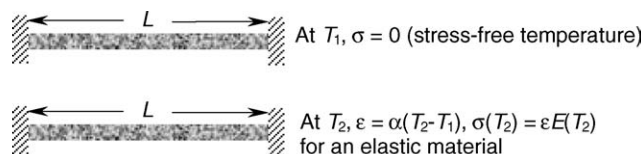

Fig. 1. For an elastic bar constrained at both ends and is in a stress-free state at temperature T_1, the resulting thermal stress at another temperature T_2 due to the temperature change is $\sigma(T_2) = \varepsilon E(T_2)$, where the strain $\varepsilon = \alpha \Delta T$ is caused by thermal expansion or contraction. However, for a viscoelastic material, $\sigma(T_2)$ will also depend on the rate of the temperature change and the time duration at T_2.

Based on the above consideration, the time–temperature superposition (TTS) principle was used to evaluate the viscoelastic properties of the cured no-flow underfill, since understanding its viscoelastic properties, which are both time and temperature dependent, allows one to model the package stress development more accurately. This is achieved by conducting dynamic mechanical measurements at multiple oscillation frequencies and over a wide range of isothermal temperatures. Based on the TTS spectra, master curves for both the storage and the loss moduli can be constructed with respect to a reference temperature by shifting each individual isothermal curve along the frequency axis. From this process, the shift factor as a function of temperature can also be obtained. The master curves can be used to describe the viscoelastic behavior of the no-flow underfill over a wide frequency or time range not accessible on the experimental time scale. Master curves at a different reference temperature can also be generated using the shift factor corresponding to that temperature. These results allow a more realistic modeling of the package stresses and prediction of reliability performance.

2. Experimental

2.1. Material

No-flow underfill material was provided by the material supplier. It contains hardeners, silica filler, coupling agent, fluxing agent, and other additives. The uncured underfill contains approximately 50 wt.% of silica filler according to thermogravimetric analysis. The uncured material was stored in a −40 °C freezer and was thawed for an appropriate amount of time before use. For TMA and DMA experiments, the material was cured according to the thermal profile suggested by the material supplier.

2.2. CTE measurement

The CTE of cured underfill material was determined using a Perkin-Elmer TMA-7 system. For sample preparation, approx-

imately 15 cc of the material was dispensed into an aluminum pan with a diameter of 43 mm. The material was cured at 150 °C for 1 h and at 165 °C for an additional 10 min in a nitrogen-purged oven. This two-stage cure profile was designed so that during the first stage of the cure (150 °C for 1 h), the fluxing agent is activated. Meanwhile, at that temperature, the gelation of the material occurs slowly. This provides enough time for the fluxing agent to interact with and clean the solder. The second stage (165 °C for 10 min) is used to further enhance the degree of cure of the underfill. DSC analysis on cured sample revealed no detectable exothermic signal, indicating that the material is fully cured.

TMA specimens with dimensions of approximately 7 mm × 4 mm × 4 mm were cut from the cured block, and TMA experiments were conducted along the length direction. During the TMA measurement, a small static loading force of 10 mN was used to minimize the sample deformation. In a typical TMA experiment, two heating scans were used: the specimen was first heated from room temperature to 165 °C at 10 °C/min, then it was cooled at 10 °C/min to −50 °C; after reaching temperature equilibrium at −50 °C, the sample was heated to 250 °C at 10 °C/min. The first heating scan was designed to reduce or eliminate the cure stress in the specimen while the CTE and the T_g of the material were measured during the second heating scan.

2.3. DMA

2.3.1. Temperature ramp experiments at a single frequency

Dynamic mechanical properties of the cured material were determined between −80 and 200 °C by using a Rheometrics DMTA 3e operated under rectangular tension mode. DMTA specimens were cut from the cured block, as described above. The effective sample length was kept at 22 mm, and the typical sample width was 2.2 mm, with a thickness of about 0.9 mm. During the DMTA experiment, the dynamic frequency f was kept at 1 Hz; strain control mode was used, with a dynamic strain of 0.02%; and the static force tracked the dynamic force and was kept at 115% of the dynamic force. The heating rate was 5 °C/min.

2.3.2. TTS experiments

TTS experiments were performed using a TA Instruments Q800 DMA, operated under tensile mode. The frequency sweep/temperature step method was used. During the experiment, the sample temperature was increased stepwise from 30 to 150 °C, with a step of 5 °C. At each isothermal temperature, the frequency f was scanned over three decades between 0.05 and 50 Hz with a total of 18 discrete frequencies, which were: 0.05, 0.07, 0.1, 0.2, 0.3, 0.5, 0.7, 1, 1.5, 2, 3, 5, 7, 10, 15, 20, 30, and 50 Hz. These frequencies were chosen so that they were approximately equally spaced on the logarithmic scale. At frequencies higher than 50 Hz, the measured signal becomes noisy or unstable at $T > 150$ °C, where the mechanical strength of the sample decreases significantly. The dynamic strain was kept at 0.04% and the static force was kept as 125% of the dynamic force. From the measured spectra of the moduli, the master curves were constructed by shifting the isothermal curves horizontally with respect to an arbitrarily selected reference temperature along the frequency axis. A small vertical shift was also necessary for constructing the master curves.

2.3.3. Stress relaxation

Stress relaxation experiments were also performed at 100 °C using a TA Instruments Q800 DMA under tensile mode. After loading the specimen at room temperature, the sample was heated to 100 °C inside the DMA furnace and stabilized at that temperature for 10 min. Then, a constant strain of $\varepsilon_o = 0.1\%$ was applied to the sample. The resulting stress $\sigma(t)$ was monitored for 30 min. The relaxation modulus $E(t) = \sigma(t)/\varepsilon_o$ can then be obtained from the stress relaxation experiments and compared with the results calculated based on the TTS experimental results.

3. Results and discussion

3.1. Thermal expansion behavior

Fig. 2 plots the relative increase in sample length and the CTE as a function of temperature. It is clear from the TMA data that below 80 °C, CTE has a weak linear dependence on temperature. When the temperature reached about 85 °C, the CTE value increased rapidly, indicating the beginning of the glass transition. At the same time, the relative sample length vs. temperature curve started to develop an inflection point, which can be taken as T_g. Based on this curve, the T_g of this material was determined to be 97 °C. Between 0 and 50 °C, the average CTE (α_1) was calculated to be ∼36.4×10^{-6} K^{-1}; between 150 and 200 °C, the CTE (α_2) was ∼137.5×10^{-6} K^{-1}. Repeated measurements confirmed that the results for α_1 and T_g are very consistent, although α_2 showed somewhat larger variation (128–140 × 10^{-6} K^{-1}), which is not well understood yet.

3.2. Dynamic mechanical properties

Fig. 3 plots the storage modulus (E'), the loss modulus (E''), and the loss tangent (tan δ) as a function of temperature. At room

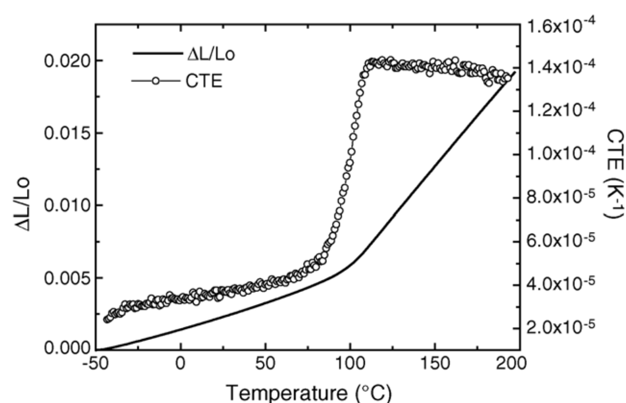

Fig. 2. Relative increase in sample length ($\Delta L/L_o$) and CTE of a cured no-flow underfill material as a function of temperature. L_o is the initial sample length at −50 °C. The heating rate was 5 °C/min. These curves were obtained from the second heating scan.

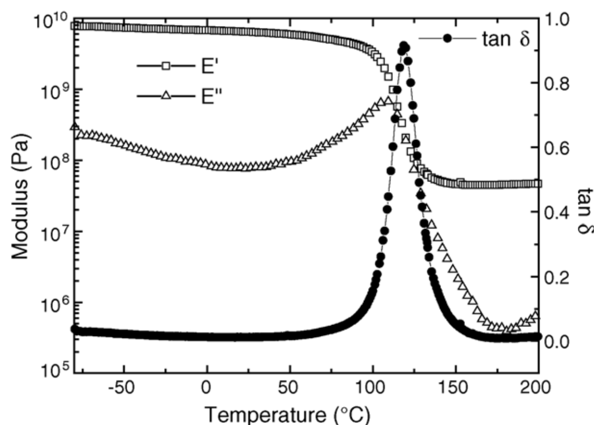

Fig. 3. Dynamic mechanical properties of a cured no-flow underfill material as a function of temperature at $f = 1$ Hz.

temperature, the storage modulus was about 6.5 GPa. When the temperature increased to ∼97 °C, E' started to decrease rather rapidly, indicating the glass transition. The glass transition range determined from the E' curve is very similar to that determined from the TMA results ($\Delta L/L_o$ versus T). When the temperature reached ∼119 °C, tan δ attained a peak value, and this temperature can also be taken as the T_g of the cured underfill.

3.3. Time–temperature superposition

Both the CTE and the modulus values of the no-flow underfill material are important for predicting the package stresses induced by the CTE mismatch among different assembly materials. An additional important consideration is the viscoelastic nature of the polymer-based underfill material, i.e. it undergoes mechanical relaxation which depends on both time and temperature. When modeling the package stress, it is necessary to consider the mechanical relaxation behavior of the underfill. The viscoelastic behavior of the underfill can be analyzed using the TTS principle, which is based on the empirical observation that the viscoelastic behavior of polymer materials at temperature T_o can be related to that at another temperature T by changing the experimental time or frequency scale [15–17]:

$$E(t, T_o) = E(a_T t, T), \tag{1}$$

or

$$E(\omega, T_o) = E\left(\frac{\omega}{a_T}, T\right), \quad \text{or} \quad E(a_T\omega, T_o) = E(\omega, T) \tag{1a}$$

where E can be the relaxation modulus, the storage modulus, or the loss modulus, t is time, ω (= $2\pi f$) is the angular frequency, and $\log a_T$ is a horizontal shift factor along the time or frequency axis (when plotted on the logarithmic scale). The physical meaning of Eq. (1a) is clear: the modulus determined at temperature T and frequency ω is equivalent to the modulus determined at a reference temperature T_o and at a shifted frequency $a_T\omega$. Generally speaking, for many polymer materials within 50 °C of the glass transition temperature, the shift factor $\log a_T$ was found to approximately follow the Williams–Landell–Ferry (WLF) equation [16,17]:

$$\log a_T = -\frac{C_1(T - T_o)}{C_2 + (T - T_o)}, \tag{2}$$

where C_1 and C_2 are constants, T_o is the reference temperature, which is often taken as the glass transition temperature, T_g. In this equation, $\log a_T$ is positive when $T < T_o$ and negative when $T > T_o$.

At low temperatures, the relaxation process is slow and requires longer time for experimental observation; at high temperatures, it is fast and takes a shorter time for experimental measurement. Therefore, the TTS principle assumes that changing the experimental temperature has the same effect as changing the relaxation time. Using the TTS experimental results, it is possible to construct a master curve at an arbitrary reference temperature which extends the mechanical measurements (modulus, compliance, etc.) beyond the range of laboratory scale in either the time or the frequency domain. This is important for accurately modeling the package stress because it allows one to consider the time-dependence of the mechanical response of the underfill material. For example, one of the reliability tests requires that all assembled devices be cycled between −55 and 135 °C, with a duration time of 15 min at each end. Thus, not only does one need to know the modulus of the underfill as a function of temperature at a single frequency, but it is also critical to understand the effect of time at these temperature limits.

Fig. 4 shows the results from a representative TTS experiment, where E', E'', and tan δ obtained during the frequency sweep measurement were plotted as a function of isothermal temperature. As frequency increases, the glass transition region increases to higher temperature, as expected.

Fig. 5 is the TTS plot showing the frequency dependence of the storage modulus at different isothermal temperatures. Based on this figure, a modulus curve determined at a pre-selected reference temperature (e.g. 100 °C) can be extended to a lower frequency range by shifting the higher temperature modulus curves to the left along the frequency axis, and vice versa. Thus, a master curve can be constructed for that reference temperature over an extended frequency range.

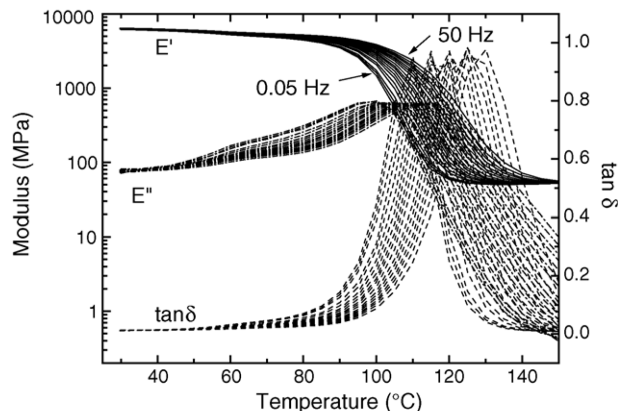

Fig. 4. Storage modulus (E'), loss modulus (E''), and loss tangent (tan δ) curves obtained from a TTS measurement carried out under tensile geometry using frequency sweep/temperature step mode. The frequency spans from 0.05 to 50 Hz.

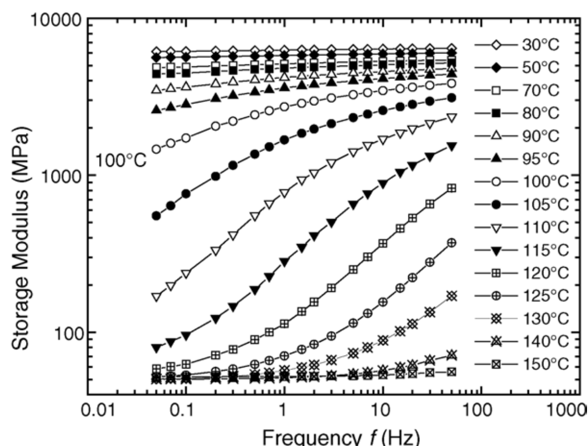

Fig. 5. Frequency dependence of the storage modulus of a cured no-flow underfill at different isothermal temperatures.

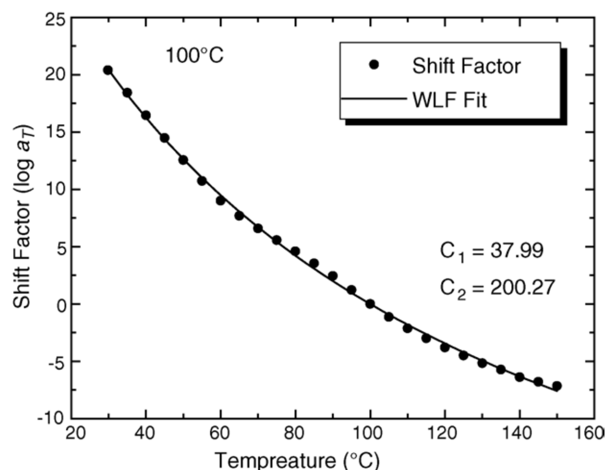

Fig. 7. Horizontal shift factor ($\log a_T$) vs. temperature for a reference temperature of $T_o = 100\,°C$. The WLF equation can fit the shift factors quite well.

3.4. Master curves and shift factors

Based on the results presented in Fig. 5, the master curves for the storage and loss moduli, and the loss tangent, were constructed with respect to a reference temperature of $T_o = 100\,°C$, as shown in Fig. 6. This reference temperature was chosen because it is close to the T_g determined in TMA experiments.

Based on the DMA results shown in Fig. 3, at $f = 1$ Hz, E' starts to decrease rather rapidly when the temperature approaches 97 °C. Thus, at $T_o = 100\,°C$, the material is expected to go through the glass transition when f approaches 1 Hz or ωa_T (note $a_{100\,°C} = 1$) approaches 2π rad/s, which is indeed the case according to Fig. 6. In fact, based on the master curves shown in Fig. 6, when $\omega a_T > 20$ rad/s, the no-flow underfill still behaves very much like a glassy solid without a significant reduction in E'. Indeed, at $\omega a_T = 20$ rad/s, E′ is about 3.1 GPa. On the other hand, at $\omega a_T < 10^{-4}$ rad/s, the cured no-flow underfill behaves like a rubbery material with E' decreases to below 50 MPa.

Master curves can be generated with respect to various reference temperatures once the shift factors are known. Once the master curves are obtained, the mechanical relaxation behavior at these temperatures for a given experimental time scale can be taken into consideration in predicting the package stresses.

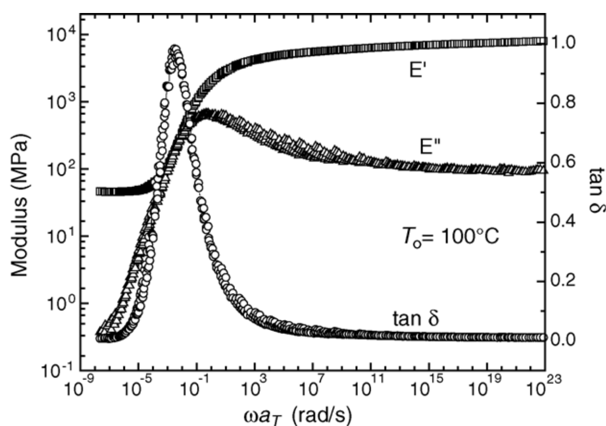

Fig. 6. Master curves generated by shifting the storage (E'), the loss (E'') moduli, and the loss tangent curves using the TTS principle with respect to a reference temperature of 100 °C.

Fig. 7 plots $\log a_T$ as a function of temperature for a reference temperature of $T_o = 100\,°C$. Within the experimental temperature range, the WLF equation given in Eq. (2) can be used to fit the shift factor data rather well, as shown in Fig. 7. The fitting parameters are $C_1 = 37.99$ and $C_2 = 200.27$ (°C or K). These results deviate from the typical “universal” values of $C_1 = 17.44$ and $C_2 = 51.60$ [16,17] when T_g is selected as the reference temperature. In fact, C_1 and C_2 do vary from polymer to polymer, especially for C_2, where large deviation from the “universal” value has been observed in many polymer systems, and it is often attributed to specific character of the polymer system [18]. In addition, values of C_1 and C_2 depend strongly on the choice of T_o: a small variation in T_o can cause large deviation from the “universal” values [19].

In the superposition of individual isothermal curves, it is often necessary to incorporate a small vertical shift factor a_V [15]:

$$E(a_T\omega, T_o) = a_V E(\omega, T), \tag{3}$$

where a_V relates to the change of material density at the experimental temperature. Fig. 8 plots the vertical shift factors as a function of temperature obtained during the superposition process at $T_o = 100\,°C$. Based on the molecular theory of viscoelasticity, Ferry et al. [16] suggested that a small vertical shift factor should be incorporated in the TTS process [15,17]:

$$a_V = \frac{\rho_o T_o}{\rho T} = \frac{V T_o}{V_o T}, \tag{4}$$

where ρ_o and ρ are material density at T_o and T, respectively; V_o and V are volume at T_o and T, respectively. In Eq. (4), T and T_o are in Kelvin. For an isotropic material, a_V can be calculated using the thermal expansion results from TMA experiments:

$$a_V = \frac{L T_o}{L_o T}. \tag{4a}$$

The calculated and experimentally determined vertical shift factors were plotted together in Fig. 8. It can be seen that the calculated values were in excellent agreement with the ones

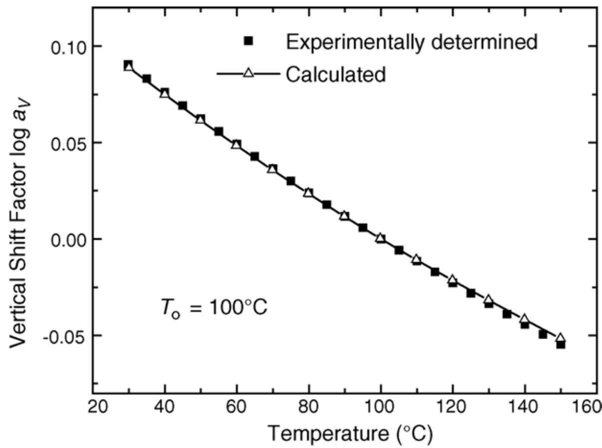

Fig. 8. Experimentally determined and calculated vertical shift factors for $T_o = 100\,°C$.

obtained experimentally through the TTS procedure. It is interesting to note that although a_V is a function of the sample length L, the plot of a_V versus T showed no signature of T_g, as revealed in Fig. 8. This can be explained by a close examination of the TMA results presented in Fig. 2. Based on the TMA data, across the entire glass transition region, which occurs approximately between 77 and 110 °C, the sample length increases by less than 0.3%. On the other hand, the increase in the absolute temperature is more than 9%. Therefore, the effect of the change in sample length on a_V is masked and over-compensated by the increase in temperature, and the T_g effect on a_V becomes undetectable.

In Fig. 9, a portion of the master curve for the storage modulus E' at $T_o = 100\,°C$ was plotted as a function of shifted frequency $a_T f$ together with the experimental data determined from individual isothermal measurement. As expected, the master curve lies on top of the isothermal data obtained at $T = 100\,°C$. To demonstrate the TTS principle, the data obtained at 120 °C was shifted horizontally by applying a shift factor of $\log a_T = -3.791$ or $a_T = 1.618 \times 10^{-4}$, as well as a small vertical shift factor of $a_V = 0.9491$. The result is the thick solid line which forms a low frequency portion of the master curve at $T_o = 100\,°C$. After shifting the data obtained at 120 °C with respect to T_o, we are able to extend the lowest frequency to 8.1×10^{-6} Hz, while the original experiment was performed at a lowest frequency of 0.05 Hz.

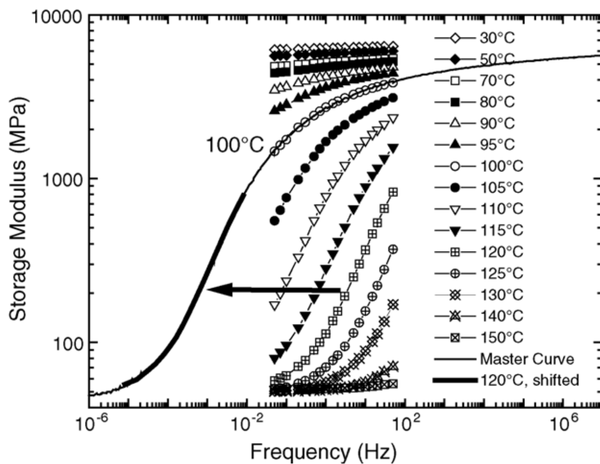

Fig. 9. Demonstration of the TTS principle: a portion of the master curve for E' at $T_o = 100\,°C$ (thin solid line) plotted as a function of $a_T f$, together with the raw experimental data obtained at various isothermal temperatures (same as Fig. 5). Thick solid line represents the E' curve at 120 °C after a horizontal shift ($a_T = 1.618 \times 10^{-4}$ or $\log a_T = -3.791$) and a small vertical shift ($a_V = 0.9491$ or $\log a_V = -0.02268$).

3.5. Relaxation modulus

In the actual process of modeling package stresses using a finite element analysis technique, it is often necessary to know the relaxation modulus in the time domain based on the master curves obtained in the frequency domain. This is because given the relaxation modulus and the history of the applied strain, the stress can be determined as [15,20]:

$$\sigma(t) = \int_{-\infty}^{t} E(t-\tau)\frac{\partial \varepsilon(\tau)}{\partial \tau}\,d\tau. \quad (5)$$

In Eq. (5), E is the relaxation modulus and is also called the stress relaxation modulus, ε is the strain, and σ is the stress. In a stress relaxation experiment, a constant strain $\varepsilon = \varepsilon_o$ is applied in the beginning of the test, then at time t after that, σ and E are simply related by [20]:

$$\sigma(t) = \varepsilon_o E(t). \quad (6)$$

From an oscillatory DMA experiment, one can obtain the real and the imaginary part of the complex modulus, $E'(\omega)$ and $E''(\omega)$. Then, the relaxation modulus can be expressed in terms of $E'(\omega)$ and $E''(\omega)$ [20,21]:

$$E(t) = \frac{2}{\pi}\int_{0}^{\infty} \frac{E'(\omega)}{\omega}\sin \omega t\,d\omega, \quad (7)$$

and

$$E(t) = \frac{2}{\pi}\int_{0}^{\infty} \frac{E''(\omega)}{\omega}\cos \omega t\,d\omega. \quad (8)$$

Several approximated equations can be used to estimate $E(t)$. The one proposed by Schwarzl and Struik is given by [21,22]:

$$E(1.25t) = E'(\omega) - 0.5303E''(0.5282\omega) - 0.021E''(0.085\omega) + 0.042E''(6.37\omega), \quad (9)$$

where $\omega = 1/t = 2\pi f$, E' and E'' were the master curves determined in the frequency domain, as shown in Fig. 6.

Another expression of $E(t)$ was suggested by Ninomiya and Ferry [23,24]:

$$E(t) = E'(\omega) - 0.4E''(0.4\omega) + 0.014E''(10\omega). \quad (10)$$

The calculated relaxation modulus for $T = 100\,°C$ using Eq. (9) was plotted in Fig. 10(a). From Fig. 10(a), we can see that when $t > 4000$ s, $E(t)$ becomes essentially a constant, which is 0.05 ± 0.01 GPa, which is the equilibrium or relaxed modulus at this temperature. In Fig. 10(a), the relaxation modulus data calculated using Eq. (10) were also plotted, and they agree very well with the results obtained using Eq. (9).

Another approach to construct the master curve for $E(t)$ in the time domain is to conduct stress relaxation experiments at

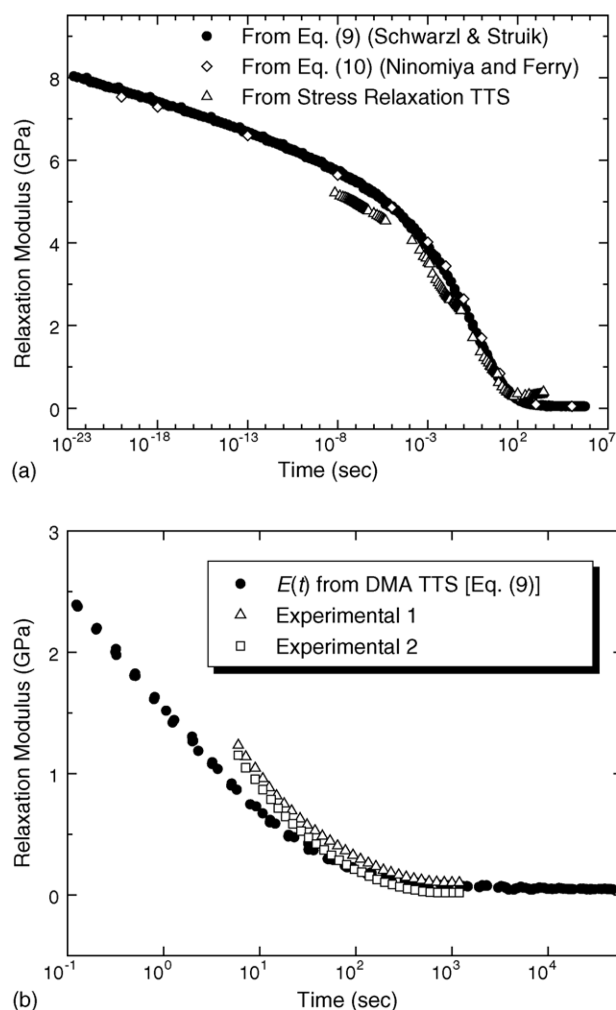

Fig. 10. (a) Relaxation modulus determined using Eq. (9) (solid circles) plotted in the time domain for $T_o = 100\,^\circ$C. Open diamonds are the relaxation modulus calculated using Eq. (10). Open triangles are the master curve constructed based on the stress relaxation TTS experiments conducted under uniaxial tensile mode [25] and (b) Solid circles: relaxation modulus determined at $T_o = 100\,^\circ$C from the oscillatory DMA TTS experiments (calculated using Eq. (9)). Open triangles and open squares: relaxation modulus determined from two independent stress relaxation experiments performed at 100 °C using DMA.

various isothermal temperatures. At each temperature, the stress relaxation modulus E is measured as a function of time. A master curve for $E(t)$ in the time domain can be constructed by shifting each isothermal curve of E versus t with respect to a reference temperature, using the same TTS principle. Such stress relaxation TTS experiments have been performed using an MTS machine under uniaxial tensile mode [25]. The obtained master curve, as shown in Fig. 10(a), was in good agreement with the one constructed through the oscillatory DMA TTS experiments. As revealed in Fig. 10(a), it seems that on a similar experimental time scale, the master curve obtained using the oscillatory DMA TTS results spans a wider range in the time domain than the one constructed from the stress relaxation TTS experiments. On the other hand, the advantage of using the stress relaxation TTS approach is that the master curve for $E(t)$ can be obtained directly by shifting the experimental data in the time domain, without going through the conversion process.

In Fig. 10(b), the relaxation modulus data obtained from the DMA stress relaxation experiments were plotted together with the relaxation modulus calculated using Eq. (9), which was based on the TTS approach. Not surprisingly, only a small portion of the calculated spectrum can be obtained experimentally. The experimentally obtained relaxation modulus data, which were from two independent measurements on two different samples, showed fairly good agreement with the calculated results. The discrepancy between the experimental data and the calculated results at $t \leq 20$ s may be caused by a small variation in the isothermal temperature, because at $T = 100\,^\circ$C, both $E(t)$ and $E'(\omega)$ are highly sensitive to temperature.

The obtained relaxation modulus, together with the obtained shift factors, are crucial for incorporating the viscoelastic behavior of the no-flow underfill in modeling the package stresses. When this is done, one can consider the effects of the temperature variation and the time scale involved in such temperature change on package thermal stresses.

TTS principle is a powerful technique for investigation relaxation behavior over a wide time or frequency range not attainable in an experimental time scale. Not only has it been widely used to study the mechanical behavior of many polymers, it has also been used recently to study the mechanical relaxations of bulk amorphous alloys [26].

Finally, we would like to point out that the TTS principle is usually true for thermorheologically simple materials. TTS may not hold if the dominant relaxation process (α relaxation) is interfered by an additional minor relaxation (β relaxation). TTS violation has been observed in other cases, for example, for non-polymeric viscous liquids in the very high viscosity regime, TTS often breaks down [27]. From the DMA results presented in Fig. 3, the cured no-flow underfill material showed no sign of secondary relaxation in the temperature range of the TTS measurement (i.e., 30–150 °C). Subsequent analysis of experimental data suggests that TTS principle is obeyed between at least 30–150 °C. In this temperature range, the horizontal shift factor data can be fitted to the WLF equation. Above 150 °C, a_T starts to deviate from the WLF equation.

4. Conclusions

In this work, thermomechanical and viscoelastic properties of a cured no-flow underfill material for flip-chip applications were characterized. TMA results showed that the cured sample goes through a glass transition near 97 °C. The average CTE between 0 and 50 °C was about $36.4 \times 10^{-6}\,\mathrm{K}^{-1}$; between 150 and 200 °C, it was $137.5 \times 10^{-6}\,\mathrm{K}^{-1}$.

DMA experiments conducted at $f = 1$ Hz revealed that at room temperature, the storage modulus of the cured material was about 6.5 GPa, which is typical for an underfill containing about 50 wt.% filler. The tan δ curve developed a single peak at 118.6 °C. At 150 °C, E' decreased to ∼46 MPa.

DMA time–temperature superposition experiment was conducted between 30 and 150 °C with the frequency scanned between 0.05 and 50 Hz. Based on the TTS data, master curves with a frequency span of 31 decades were constructed for E' and E'' at a reference temperature of 100 °C. The horizontal

and the vertical shift factors were determined based on the TTS results. The master curve for the relaxation modulus at 100 °C was also determined from the TTS data, and the results are in good agreement with the data obtained from the stress relaxation experiments. With the WLF shift factors, the master curves for the relaxation modulus can be determined at other temperatures. The determined master curves for the relaxation modulus, together with the thermal expansion behavior of the no-flow underfill material, provided crucial material properties for modeling package stresses.

Acknowledgements

I would like to thank Fred Cardona, Stacy Nakamura, and Alan Overson of Intel Corporation for providing experimental assistance during the course of this study; and Dr. Tom Miller (Intel Corporation) for carefully reviewing this manuscript. I have benefited from many discussions with Drs. S. H. Shi, Ibrahim Bekar and Prasanna Raghavan (all from Intel Corporation) on no-flow underfill technology and on incorporating the viscoelastic properties of packaging materials into modeling the package stresses using finite element analysis approach. Special appreciation goes to Dr. Ibrahim Bekar for calculating the master curve for $E(t)$ using Eq. (9), and for sharing the master curve based on the stress relaxation TTS experiments. Finally, I would like to thank Mr. Steve Page and Dr. Terri (Tianhong) Chen from TA Instruments for useful discussions on conducting the TTS experiments.

References

[1] E.M. Davis, W.E. Harding, R.S. Schwartz, J.J. Corning, Solid logic technology: versatile, high-performance microelectronics, IBM J. Res. Dev. 8 (1964) 102–114.
[2] J.H. Lau (Ed.), Flip Chip Technologies, McGraw-Hill, New York, 1995.
[3] Y. Tsukada, Y. Mashimoto, T. Nishio, N. Mii, Reliability and stress analysis of encapsulated flip chip joint on epoxy based printed circuit packaging, in: W.T. Chen, Abe Hiroyuki (Eds.), Proceedings of the 1992 Joint ASME/JSME Conference on Electronic Packaging, vol. 2, Materials and Processes, Reliability, Quality Control and NDE, American Society of Mechanical Engineers, New York, 1992, pp. 827–835.
[4] S.C. Machuga, S.E. Lindsey, K.D. Moore, A.F. Skipor, Encapsulation of flip-chip structure, in: Proceedings of the 13th IEEE/CHMT International Electronics Manufacturing Technology Symposium, 1992, pp. 53–58.
[5] C.A. Harper (Ed.), Electronic Packaging and Interconnection Handbook, 2nd ed., McGraw-Hill, New York, 1997.
[6] D. Suryanarayana, R. Hsiao, T.P. Gall, J.M. McCreary, Flip-chip solder bump fatigue life enhanced by polymer encapsulation, in: Proceedings of the 40th IEEE Electronic Components and Technology Conference (ECTC), 1990, pp. 338–344.
[7] C.P. Wong, S.H. Shi, No-flow underfill of epoxy resin, anhydride, fluxing agent, and surfactant, U.S. Patent, 6,180, 696, January 30, 2001.
[8] C.P. Wong, S.H. Shi, G. Jefferson, High performance no-flow underfills for low-cost flip-chip applications, in: Proceedings of the 47th IEEE Electronic Components and Technology Conference (ECTC), 1997, pp. 850–858.
[9] C.P. Wong, S.H. Shi, G. Jefferson, High performance no-flow underfills for low-cost flip-chip applications: material characterization, IEEE Trans. Comp., Packag., Manufact. Technol. 21 (1998) 450–458.
[10] S.H. Shi, C.P. Wong, Study of the fluxing agent effects on the properties of no-flow underfill materials for flip-chip applications, IEEE Trans. Comp., Packag., Manufact. Technol. 22 (1999) 141–151.
[11] S.H. Shi, C.P. Wong, Recent advances in the development of no-flow underfill encapsulants—a practical approach towards the actual manufacturing application, IEEE Trans. Comp., Packag., Manufact. Technol. 22 (1999) 331–339.
[12] Z.Q. Zhang, S.H. Shi, C.P. Wong, Development of no-flow underfill materials for lead-free solder bumped flip-chip applications, IEEE Trans. Comp., Packag., Manufact. Technol. 24 (2001) 59–66.
[13] S.H. Shi, No-flow technology—some fundamentals, Intel Internal Report, November 2003.
[14] T. Caskey, T. Chen, S. Jayaraman, V. LeBonheur, No-flow underfill material development, Intel Assembly Test Technol. J. 6 (2003) 303–310.
[15] I.M. Ward, D.M. Hadley, An Introduction to the Mechanical Properties of Solid Polymers, John Wiley and Sons, New York, 1997.
[16] M.L. Williams, R.F. Landel, J.D. Ferry, The temperature dependence of relaxation mechanisms in amorphous polymers and other glass-forming liquids, J. Am. Chem. Soc. 77 (1955) 3701–3707.
[17] J.D. Ferry, Viscoelastic Properties of Polymers, 3rd ed., Wiley, New York, 1980.
[18] C.A. Angell, Why $C_1 = 16–17$ in the WLF equation is physical–and the fragility of polymers, Polymer 26 (1997) 6261–6266.
[19] G. Adam, J.H. Gibbs, On the temperature dependence of cooperative relaxation properties in glass-forming liquids, J. Chem. Phys. 43 (1965) 139–146.
[20] W.N. Findley, J.S. Lai, K. Onaran, Creep and Relaxation of Nonlinear Viscoelastic Materials: With an Introduction to Linear Viscoelastisity, Dover Publications, Inc., New York, 1976 (Chapter 5).
[21] F.R. Schwarzl, L.C.E. Struik, Analysis of relaxation measurements, Adv. Mol. Relaxat. Process 1 (1967) 201–255.
[22] D.J. O'Brien, P.T. Mather, S.R. White, Viscoelastic properties of an epoxy resin during cure, J. Comp. Mater. 35 (2001) 883–904.
[23] K. Ninomiya, J.D. Ferry, Some approximate equations useful in the phenomenological treatment of linear viscoelastic data, J. Colloid Sci. 14 (1959) 36–48 [Note that the term $0.14G''(10\omega)$ in Eq. (45) on p. 45 should be $0.014G''(10\omega)$].
[24] K.P. Menard, Dynamic Mechanical Analysis: A Practical Introduction, CRC Press, Boca Raton, 1999 (Chapter 7).
[25] S. Tandon, S. Sane, M. Mello, B. Chandran, G. Raiser, S. Cho, X.J. Fan, R. Harries, A. Johnson, Y. He, I. Bekar, Viscoelastic Material Characterization for Underfills, Internal report, Intel Corporation, 2004.
[26] H.T. Jeong, J.-H. Kim, W.T. Kim, D.H. Kim, The mechanical relaxations of a $Mm_{55}Al_{25}Ni_{10}Cu_{10}$ amorphous alloy studied by dynamic mechanical analysis, Mater. Sci. Eng. A 385 (2004) 182–186.
[27] N.B. Olsen, T. Christensen, J.C. Dyre, Time–temperature superposition in viscous liquids, Phys. Rev. Lett. 86 (2001) 1271–1274.